

Synthesis and spectroscopic studies of diaza-8-crown-4-dinitrophenyl ethers

Claudia Galea, Damjan Makuc, Konrad Szaciłowski, Janez Plavec & David C. Magri

To cite this article: Claudia Galea, Damjan Makuc, Konrad Szaciłowski, Janez Plavec & David C. Magri (2019): Synthesis and spectroscopic studies of diaza-8-crown-4-dinitrophenyl ethers, *Supramolecular Chemistry*, DOI: [10.1080/10610278.2019.1662420](https://doi.org/10.1080/10610278.2019.1662420)

To link to this article: <https://doi.org/10.1080/10610278.2019.1662420>

 View supplementary material 

 Published online: 10 Sep 2019.

 Submit your article to this journal 

 Article views: 9

 View related articles 

 View Crossmark data 

ARTICLE



Synthesis and spectroscopic studies of diaza-8-crown-4-dinitrophenyl ethers

Claudia Galea^a, Damjan Makuc^b, Konrad Szaciłowski^c, Janez Plavec^{b,d} and David C. Magri^a

^aDepartment of Chemistry, Faculty of Science, University of Malta, Msida, Malta; ^bSlovenian NMR Centre, National Institute of Chemistry, Ljubljana, Slovenia; ^cAcademic Centre of Materials and Nanotechnology, AGH University of Science and Technology, Kraków, Poland; ^dEN-FIST Centre of Excellence, Ljubljana, Slovenia

ABSTRACT

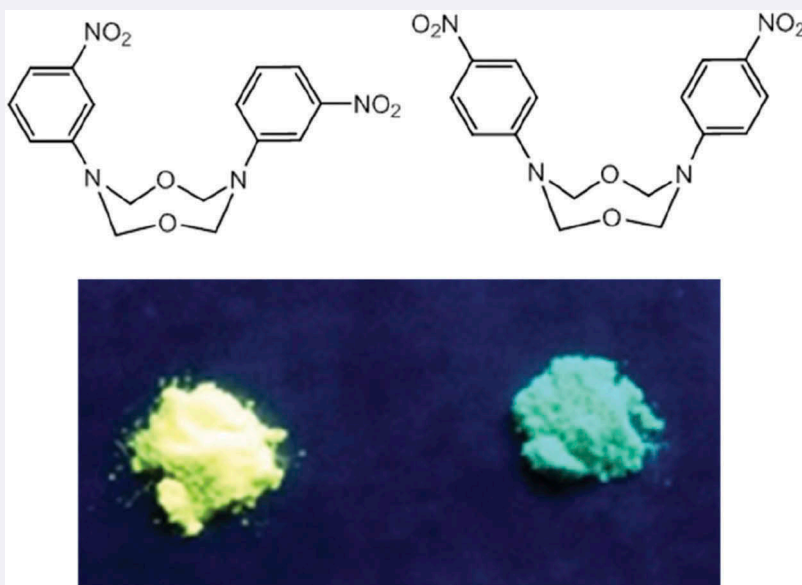
The macrocycles 3,7-*bis*(3-nitrophenyl)-1,5,3,7-dioxadiazocane **1** and 3,7-*bis*(4-nitrophenyl)-1,5,3,7-dioxadiazocane **2** were synthesised by a one-pot reaction with substituted nitroanilines and formaldehyde under acidic conditions. The same reaction with 2-nitroaniline yielded *N,N'*-(oxybis(methylene))bis(2-nitroaniline) **3** rather than 3,7-*bis*(2-nitrophenyl)-1,5,3,7-dioxadiazocane **4**. The yellow powders **1–3** were characterised by ¹H/¹³C/¹⁵N NMR, FTIR and HRMS. The photophysical properties were studied by UV-visible absorption and steady-state fluorescence spectroscopy. Acid dissociation constants were determined by UV-visible absorption titrations in 1:1 (v/v) acetonitrile/water to be 0.80 and 3.1 for the *meta*- and *para*-substituted compounds **1** and **2**, respectively. Compounds **1** and **2** were discovered to fluoresce in the solid-state, yellow and green, respectively, but not in solution. Density functional theory (DFT) calculations for **1–4** provide insight into the frontier molecular orbital energy levels. These compounds represent a new class of fluorescent heterocyclic building blocks for organic and supramolecular applications.

ARTICLE HISTORY

Received 7 May 2019
Accepted 27 August 2019

KEYWORDS

Dioxadiazocanes; macrocycle; internal charge transfer; nitrogen NMR spectroscopy; solid-state fluorescence



1. Introduction

Crown ethers (1–5) are widely used in the design of photo-responsive materials (6) biomedical applications (7) and molecular logic-based computation (8). The standard crown ethers used in sensing applications typically consist of 12 or more atoms, although examples with fewer atoms do exist. For example, a nine-atom diaza-9-crown-3 ether

was reported by Gunnlaugsson as part of a fluorescent chemosensor for Li⁺ (9, 10).

1,5,3,7-Dioxadiazocanes are a class of eight-atom heterocycle with two nitrogen and two oxygen atoms separated by methylene units. A search through the literature reveals that studies on 1,5,3,7-dioxadiazocanes (11–15) and 1,5,3,7-dithiadiazocanes (16) are rather limited to synthesis and crystallographic analysis.

They adopt a crown-like conformation with the *N*-aryl substituents on the same side of the eight-membered ring. To the best of our knowledge, there are no reported studies on the photophysical and physicochemical properties of this class of compound.

Hence, we were curious to explore whether 1,5,3,7-dioxadiazocanes may be suitable as fluorescent materials (17, 18), and perhaps, as proton and lithium chemosensors (19). A promising lead was finding from the literature that the crown cavity diameter is 3.61 Å and that the ionic diameter of Li⁺ is 1.45 Å (3). Because of the close proximity of the two nitrogen atoms, we also postulated that perhaps 1,5,3,7-dioxadiazocanes may act as proton sponges and form an N-H-N bond (20–23).

In this paper, we present our findings including the synthesis and spectroscopic studies of heterocyclic 3,7-*bis*(nitrophenyl)-1,5,3,7-dioxadiazocanes isomers **1** and **2** as internal charge transfer (ICT) chemosensors (1). The 1,5,3,7-dioxadiazocanes possess two nitrophenyl moieties according to a *chromophore-receptor-spacer-receptor-chromophore* arrangement (24, 25). We studied the compounds by UV-visible absorption, steady-state fluorescence and ¹H/¹³C/¹⁵N 2D NMR correlation spectroscopies and density functional theory (DFT) to gain insight into their physicochemical properties.

2. Experimental

2.1. Materials

Formic acid (AnalaR, BDH), formaldehyde (36.5%, Sigma-Aldrich), 1-amino-4-nitrobenzene (97%, Cambrian Chemicals), 1-amino-3-nitrobenzene (BDH), 1-amino-2-nitrobenzene (96%, Cambrian Chemicals), tetrahydrofuran (99.9%, Sigma-Aldrich), lithium perchlorate (99%, Hopkin & Williams Ltd), acetonitrile (99.9%, Sigma-Aldrich), methanol (99.9%, Sigma-Aldrich), chloroform (99.9%, Fisher Scientific) and dimethyl sulfoxide (99.9 atom D%, Acros Organics) were used as received.

2.2. Instrumentation

Ultraviolet-visible absorption spectra were measured with a Jasco V-650 spectrophotometer at a scan speed of 200 nm min⁻¹ between 200 and 500 nm. Steady-state fluorescence spectra were recorded on a Jasco FP-8300 fluorescence spectrometer as solid samples on glass slides positioned at 45 degrees to the incident excitation wavelength. pH measurements were performed with a Hanna Instruments 210 pH metre calibrated with pH 4.0 and 7.0 buffers. ¹H and ¹³C NMR spectra were initially measured with a Bruker AM250 NMR spectrometer fitted with ¹H/¹³C 5 mm dual probe at 250.1 and 62.9 MHz using

a Bruker Aspect 3000 computer. Tetramethylsilane (TMS) was used as the internal reference for ¹H NMR (δ0.00 ppm). NMR samples were taken at 298 K using 5–10 mg of sample dissolved in 0.8 mL of DMSO-*d*₆. Chemical shifts are reported in parts per million downfield of TMS. Heteronuclear Multiple Bond Correlation (HMBC) spectra were recorded on a DD2 Agilent Technology at frequencies of 599.66 MHz and 60.78 MHz for ¹H and ¹⁵N NMR, respectively. Chemical shifts are referenced to the residual solvent signal of DMSO-*d*₆ while ¹⁵N chemical shifts were referenced relative to ammonia (δ0.00 ppm). ¹³C NMR spectra were recorded at a frequency of 150.8 MHz. FTIR spectra were recorded as KBr discs with dried potassium bromide on a Shimadzu IRAffinity-1 spectrophotometer calibrated using 1601 cm⁻¹ polystyrene absorption peak. Low-resolution mass spectra were acquired by a triple quadrupole mass spectrometer-TQD mass spectrometer (Waters Ltd. UK) equipped with an Acquity UPLC and an electrospray ion source. High-resolution mass spectra were obtained with a quadrupole time-of-flight instrument-Xevo QToF mass spectrometer (Waters Ltd. UK) equipped with atmospheric pressure gas chromatography (APGC) and solids analysis probe (ASAP). Melting points were obtained using a Stuart melting point apparatus.

2.3. Synthesis

2.3.1. Synthesis of 3,7-*bis*(3-nitrophenyl)-1,5,3,7-dioxadiazocane **1**

The *meta*-substituted product was synthesised using a literature procedure (12). 1.4 g (10 mmol) of 3-nitroaniline and 20 μL (0.025 g, 0.55 mmol) of formic acid were dissolved in 50 mL of acetonitrile in a 100 mL round-bottomed flask. After dissolution, 1.2 mL (1.2 g, 15 mmol) of formaldehyde was added. The reaction mixture was stirred at room temperature for 24 h. A yellow powder was collected by suction filtration and washed with cold acetonitrile in 80% yield (1.08 g). m.p. 226–227°C; ¹H NMR (250 MHz, DMSO-*d*₆, ppm): 4.90–5.60 (br s, 8H), 7.00–7.60 (m, 8H); ¹³C NMR (63 MHz, DMSO-*d*₆, ppm): 81.4, 109.0, 112.8, 121.0, 129.9, 145.1, 147.8; IR (KBr, ν_{max}, cm⁻¹): 3110, 2972, 2935, 2885, 1602, 1525, 1350, 1136, 1028, 950, 870, 848, 725; UV-vis (1:1 (v/v) MeCN:H₂O, λ_{max}/nm (log ε)): 370 (3.50); UV-vis (MeCN, λ_{max}/nm (log ε)): 367 (3.38); HRMS (ESI-TOF): m/z Calc. for C₁₆H₁₇N₄O₆ [M + H] 361.1156, found 361.1156.

2.3.2. Synthesis of 3,7-*bis*(4-nitrophenyl)-1,5,3,7-dioxadiazocane **2**

The *para*-substituted product was synthesised using a similar procedure with 4-nitroaniline (12). Recrystallisation from THF resulted in a yellow powder

in 65% yield (0.90 g). m.p. 256–258°C; ^1H NMR (250 MHz, $\text{DMSO-}d_6$, ppm): 4.90–5.80 (br s, 8H), 6.95 (d, $J = 9.4$ Hz, 4H), 7.86 (d, $J = 9.4$ Hz, 4H); ^{13}C NMR (63 MHz, $\text{DMSO-}d_6$, ppm): 81.6, 114.1, 124.3, 138.5, 150.0; IR (KBr, ν_{max} , cm^{-1}): 3116, 3090, 2950, 1597, 1508, 1323, 1303, 1030, 990, 933, 890, 750; UV-vis (1:1 (v/v) MeCN:H₂O, λ_{max} /nm (log ϵ): 351 (4.53); (MeCN, λ_{max} /nm (log ϵ): 346 (4.45); HRMS (ESI-TOF): m/z Calc. for $\text{C}_{16}\text{H}_{17}\text{N}_4\text{O}_6$ [M + H] 361.1156, found 361.1133.

2.3.3. Synthesis of *N, N'*-(oxybis(methylene))bis(2-nitroaniline) **3**

The product was synthesised using a similar procedure with 2-nitroaniline (**12**). Recrystallisation from THF resulted in a yellow powder in 49% (0.67 g). m.p. 176–178°C; ^1H NMR (250 MHz, $\text{DMSO-}d_6$, ppm): 4.90 (d, $J = 6.6$ Hz, 4H), 6.80 (t, $J = 6.7$ Hz, 2H), 7.20 (d, $J = 8.7$ Hz, 2H), 7.50 (t, $J = 7.1$ Hz, 2H), 8.10 (d, $J = 8.7$ Hz, 2H), 8.80 (br t, $J = 6.5$ Hz, 2H); ^{13}C NMR (63 MHz, $\text{DMSO-}d_6$, ppm): 69.0, 115.6, 116.8, 125.7, 132.3, 135.8, 143.5; IR (KBr, ν_{max} , cm^{-1}): 3401, 3084, 1614, 1506, 1345, 1271, 1170, 1030, 1006, 890, 746; UV-vis (1:1 (v/v) MeCN:H₂O, λ_{max} /nm (log ϵ): 406 (4.12); UV-vis (MeCN, λ_{max} /nm (log ϵ): 402 (4.09); HRMS (ESI-TOF): m/z Calc. for $\text{C}_{14}\text{H}_{14}\text{N}_4\text{O}_5\text{Na}^+$ 341.0856, found 341.0858.

2.4. pH and metal ion titrations

UV-visible absorption titrations were carried out as a function of proton concentration with 50 μM solution of **1–3** in 50 mL of 1:1 (v/v) acetonitrile/water. Stock solutions were prepared by dissolving *ca.* 10 mg of sample in 100 mL of acetonitrile and diluting with 1:1 (v/v) acetonitrile/water to the appropriate absorbance. The acid dissociation constants ($\text{p}K_{\text{a}}$) were determined from absorbance-pH plots and fitted to a linearised Henderson-Hasselbalch equation adapted for spectroscopic measurements (eq.(1)) (26):

$$\log\left(\frac{A_{\text{max}} - A}{A - A_{\text{min}}}\right) = \text{pH} - \text{p}K_{\text{a}} \quad (1)$$

where A_{max} and A_{min} are the maximum and minimum peak absorbances, A is the absorbance at the specific

pH and $\text{p}K_{\text{a}}$ is the negative logarithm of acid dissociation constant.

2.5. DFT computations

The ground and excited states electronic structure was computed with the GAUSSIAN09 E.01 software package (27). Hybrid DFT was employed within the Coulomb-attenuated method, CAM-B3LYP exchange–correlation functional (28), 6–311 + g(d,p) basis functions and a def2tzv fitting set. Unconstrained optimisation of the molecular geometry was carried out until the total energy converged to 10 – 8 Hartree in the self-consistent electronic loop. Electronic transitions were computed using time-dependent DFT method using the same functional and basis sets as for geometry optimisation. Electronic absorption spectra were calculated assuming the spectral bandwidth of 0.333 eV.

2.6. Solid-state fluorescence studies

Solid-state fluorescence measurements were done on solid samples placed between two glass microscope slides. The slides were set at a 45° angle to the excitation and emission slits. The excitation wavelength was set at 370 nm, 351 nm and 406 nm for **1–3**, respectively, and scanned from 450 to 600 nm. The excitation and emission slits were set at 5.0 nm. Measurements were background corrected.

3. Results and discussion

3.1. Synthesis and characterisation

The 3,7-di(nitrophenyl)-1,5-dioxo-3,7-diazacyclooctanes were synthesised by a one-pot reaction using the procedure by Kakanejadifard (Figure 1) (11). The 2-, 3- and 4-nitroanilines were reacted with formaldehyde in formic acid (**12**). 3,7-bis(3-nitrophenyl)-1,5,3,7-dioxadiazocane **1** and 3,7-bis(4-nitrophenyl)-1,5,3,7-dioxadiazocane **2** were obtained in 80% and 65% yield as yellow powders. The solids are readily soluble in DMSO, acetonitrile and 1:1 (v/v) acetonitrile/water and insoluble in water, methanol,

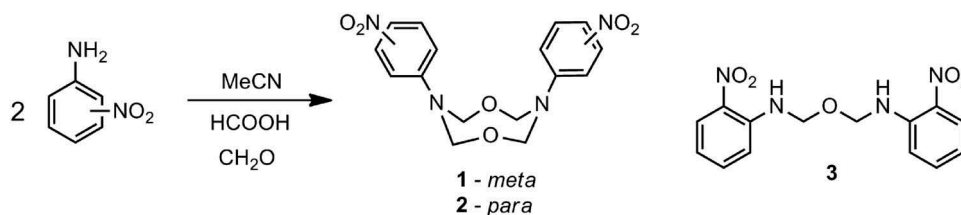


Figure 1. The one-pot syntheses of **1–3**.

ethanol, acetone, chloroform and dichloromethane. The reaction with 2-nitroaniline yielded *N, N'*-(oxybis(methylene))bis(2-nitroaniline) **3** in 49% yield rather than 3,7-bis(2-nitrophenyl)-1,5,3,7-dioxadiazocane **4**. The compounds were characterised by $^1\text{H}/^{13}\text{C}/^{15}\text{N}$ NMR, IR, HRMS (See experimental and Figures S1-S12).

The ^1H NMR spectrum of the *meta*-substituted **1** in DMSO- d_6 shows a broad signal at 5.3 ppm corresponding to the eight methylene protons of the macrocycle (Figure S1). The complex splitting pattern between 7.1 ppm and 7.6 ppm for the aromatic proton resonances is due to second-order coupling effects. A 1:1 integration ratio is calculated between the area of the broad singlet and the total area under the aromatic peaks. The ^1H NMR spectrum of the *para*-substituted **2** has a broad signal at 5.3 ppm and two doublets at 6.95 ppm and 7.86 ppm, which is typical of an AB quartet splitting pattern and an integration ratio of 1:1:2 (Figure S3). The ^{13}C NMR spectrum of **1** reveals seven magnetically non-equivalent carbon atoms (Figure S2), while the spectrum of **2** shows five different carbon atoms (Figure S4). The mass spectra of **1** and **2** provide a molecular ion peak M^+ at m/z 361.1 (Figures S7-S8).

As stated previously, our attempts to prepare 3,7-bis(2-nitrophenyl)-1,5,3,7-dioxadiazocane **4** were unsuccessful, and instead we obtained *N, N'*-(oxybis(methylene))bis(2-nitroaniline) **3**. The ^1H NMR spectrum of **3** is shown in Figure S5. Four resonances are observed between 6.6 ppm and 8.2 ppm, while a sharp doublet and a broad distorted triplet appear at 4.90 ppm and 8.80 ppm, respectively. A closer analysis of the ^1H NMR revealed a signal integration ratio of 1:4:2. The IR spectrum has a strong sharp peak at *ca.* 3400 cm^{-1} (Figure S12) characteristic of N-H stretching of a secondary amine, which is absent in the IR spectra of **1** and **2** (Figures S10-11). The ^{13}C NMR spectrum of **3** reveals seven magnetically non-equivalent carbon atoms (Figure S6). The resonance at 69.0 ppm is attributed to the two methylene carbon atoms, which is significantly lower than the resonance of 81.4 ppm for the four methylene carbon atoms of **1** (Figure S2). Correlation signals in the 2D NMR spectra, which included ^1H - ^{13}C HSQC and HMBC (Figures S13-S14) allowed for the unequivocal structure elucidation of **3**. Notably, no correlation was observed for the NH resonance at 8.80 ppm in the 2D ^1H - ^{13}C HSQC. The HRMS confirmed an expected molecular ion peak M^+ at m/z 341.1 (Figure S9).

3.2. UV-vis absorption spectrophotometric studies

The UV-visible absorption spectra of **1-3** were obtained in acetonitrile (ACN) and 1:1 (v/v) ACN/water. A summary of the ground state photophysical parameters is tabulated in Table 1. In ACN peak maxima for **1-3** are observed at

Table 1. pK_a and photophysical parameters of **1-3** in 1:1 (v/v) water/acetonitrile and acetonitrile determined by UV-visible absorption spectroscopy.

Parameter	1	2	3
pK_a^a	0.80	3.1 ^b	<0 ^c
λ_{max} (1:1 MeCN/H ₂ O)/nm	370	351	406
Log ϵ ($/\text{cm}^{-1} \text{M}^{-1}$)	3.50	4.53	4.12
$\lambda_{\text{isos}}/\text{nm}$	275	282	- ^d
λ_{max} (MeCN)/nm	367	346	402
Log ϵ ($/\text{cm}^{-1} \text{M}^{-1}$) ^e	3.38 (3.44)	4.45 (4.50)	4.08 (3.77)

^aError \pm 0.10. Measurements done in duplicate. ^bBased on UV-vis data between pH 1 and 5. ^cOnly minor changes on titration to pH 0.0. ^dNo isosbestic point observed. ^eIn parentheses from simulated UV-visible spectra.

367 nm, 346 nm and 402 nm, respectively. The log ϵ are 3.38, 4.45 and 4.08 for **1-3**, respectively. In 1:1 (v/v) ACN/water there is a slight bathochromic shift of 3 to 5 nm: the peak maxima appear at 370 nm, 351 nm and 406 nm, respectively (Figure 2). The log ϵ values in 1:1 (v/v) aqueous ACN are 3.50, 4.53 and 4.12 for **1-3**, respectively. The peak shift is attributed to an $\pi\pi^*$ ICT state, which is better stabilised in the more polar solvents.

Acid-base titrations were conducted in 1:1 ACN/water (Figure 3). No significant changes were observed in the UV-visible absorption spectra above pH 5.0, hence titrations focused on the range between pH 0 and 5. Titration of **1** with acid resulted in a downward shift at 370 nm, a dramatic decrease at 230 nm and the appearance of an isosbestic point at 275 nm. These results suggest protonation occurs at an anilinic nitrogen atom site. Titration of **2** results in an increase in the peak at *ca.* 350 nm accompanied by a pronounced bathochromic shift of 25 nm up to pH 1 and followed by a decrease on addition of further acid. An isosbestic point occurs at 282 nm. The pK_a values of **1** and **2** were determined from the absorbance-pH plots fitted to the linearised Henderson-Hasselbalch (equation 1) to be 0.80 and 3.1, respectively (26). The pK_a values of 4-nitroaniline and 3-nitroaniline of 1.0 and 2.5 are of comparable magnitude to **1** and **2** suggesting there is little if any eclipsing interaction between the orbitals of the two anilinic nitrogen atoms. Compound **3** showed no significant change in the UV-visible spectra even at pH 1 (Figure S15).

The UV-visible absorption titrations of **1-3** with Li^+ in 1:1 (v/v) ACN/water showed no significant changes (Figures S16-18). Therefore, there is no clear evidence for metal ion-ligand complexation. These results are contrary to the selective nine-atom diaza-9-crown-3 ether Li^+ chemosensor by Gunnlaugsson (9, 10). The lack of complexation by **1** and **2** is postulated to be due to two possibilities: 1) the cavity size is perhaps one atom too small, and 2) one or both of the carbonyl oxygen atoms adjacent to the diaza-9-crown-3 ether assist to coordinate Li^+ .

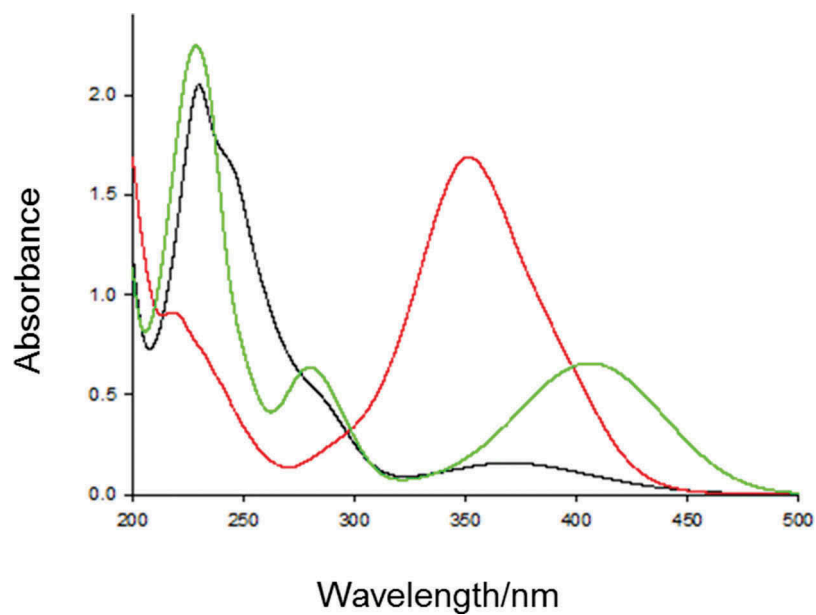


Figure 2. UV-visible absorption spectra of 50 μM **1** (black), **2** (red) and **3** (green) in 1:1 (v/v) acetonitrile/water.

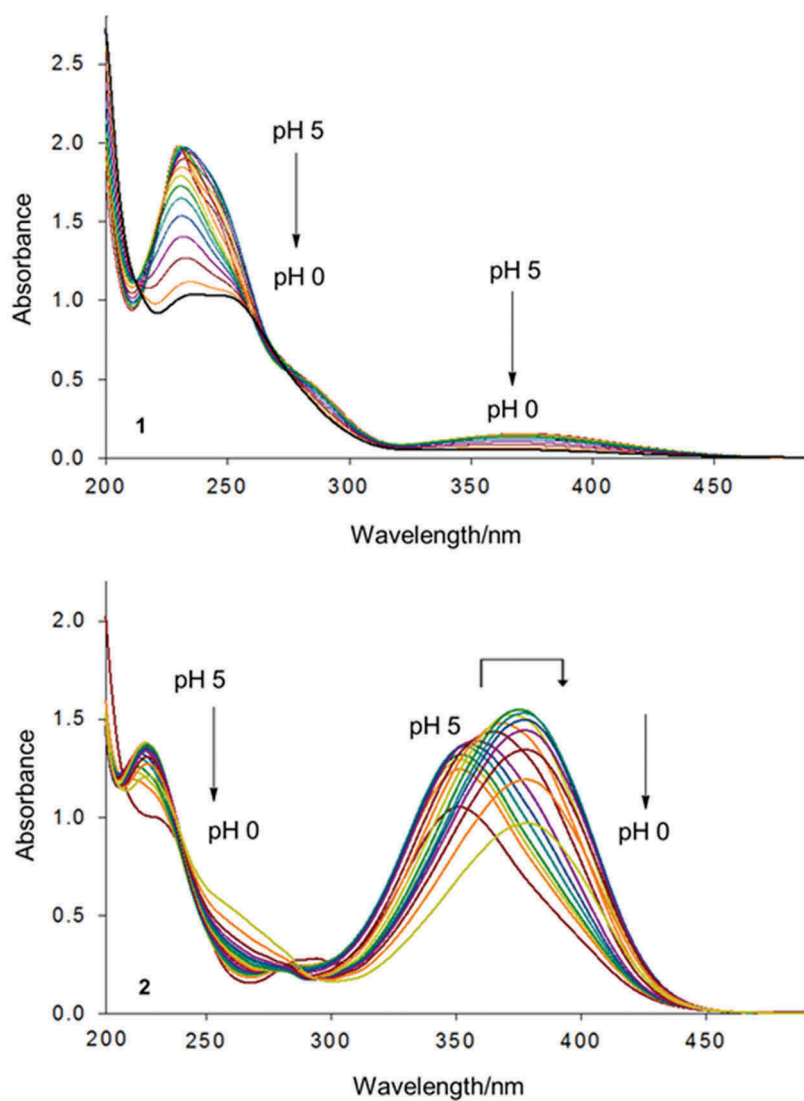


Figure 3. UV-visible absorption spectra of **1** and **2** as a function of pH in 1:1 (v/v) acetonitrile/water.

3.3. ^1H NMR titration studies

^1H NMR titrations were performed in $\text{DMSO-}d_6$ for the three compounds by adding increasing concentrations of DCI acid. Figure 4 shows a comparison of the ^1H NMR spectra of *meta*-substituted **1** at pD 7 and pD 4. Full sets of NMR titration spectra are shown in the ESI for **1–3** (Figures S19, S22 and S25). At neutral pD, compound **1** has a single set of proton resonances. However, as the concentration of acid increased, more proton resonances are observed due to 1H^+ from the protonation of an anilinic nitrogen atom. Notably, the broad peak corresponding to the methylene protons of the macrocycle at 5.3 ppm was replaced by several overlapping resonances in the region between 4.5 ppm and 6.0 ppm due to a loss of symmetry. Analogous ^1H NMR spectral changes were observed for **2** (Figure S22). Titration of **3** with DCI results in the four aromatic resonances between 6.5 ppm and 8.5 ppm splitting into eight resonances indicating a loss of symmetry due to protonation (Figure S25). The broad peak at 8.80 ppm assigned to the NH atom disappears on addition of DCI as a result of deuterium exchange.

3.4. $^1\text{H-}^{15}\text{N}$ NMR titration studies

$^1\text{H-}^{15}\text{N}$ HMBC spectra of **1–3** were obtained in $\text{DMSO-}d_6$ at pD 7 and pD 3 to better understand the protonation equilibria (29–31). The ^{15}N NMR chemical shifts are provided in Table 2 and the accompanying $^1\text{H-}^{15}\text{N}$ HMBC spectra are available in the ESI (Figures S20, S21, S23, S24, S26, S27). Two nitrogen atom resonances are observed for *meta*-substituted **1** at pD 7 attributed to the unprotonated nitrogen atoms of the anilinic and

Table 2. Select ^{15}N chemical shifts (δ) of **1–3** in $\text{DMSO-}d_6$ as a function of pD.

Compound	pD 7		pD 3	
	Anilinic	NO_2	Anilinic	NO_2
1	92	372	76, 86, 86, 89, 91, 107	372
2	102	371	76, 90, 101, 118	371
3	86	373	78, 95	373

^{15}N NMR δ were determined by $^1\text{H-}^{15}\text{N}$ correlations in gHMBC spectra.

nitro moieties at δ_{N} 92 ppm and 372 ppm, respectively (Figure S20). On addition of acid at pD 3, the same two ^{15}N chemical shifts were observed. Additional correlation signals were observed for the methylene diaza-crown ether groups of **1**, with intense peaks at δ_{N} 76, 86, 86, 89 and 107 ppm (Figure S21). Several nitrogen nuclei between 76 ppm and 107 ppm could be assigned to the anilinic moieties, tentatively corresponding to the protonated and perhaps diprotonated forms of the diaza-crown ethers. Furthermore, multiple signals were observed in the $^1\text{H-}^{15}\text{N}$ NMR spectra of **1** indicating a loss of the symmetry due to protonation of an anilinic nitrogen atom.

$^1\text{H-}^{15}\text{N}$ HMBC spectra of the *para*-nitro analogue **2** showed two nitrogen atoms at pD 7 at δ_{N} 102 ppm and 371 ppm (Figure S23). Similar to compound **1**, the increased concentration of DCI to **2** led to the detection of new resonances at pD 3 (Figure S24). In addition to unprotonated anilinic and nitro moiety atoms, three correlation signals were observed at δ_{N} 76, 90 and 118 ppm. Overlapping ^1H NMR resonances assigned to the methylene protons of the diazacrown ether moieties suggest the presence of protonated and unprotonated variants of **2** at acidic conditions. A single set of $^1\text{H-}^{15}\text{N}$ correlation signals were also observed for **3** at pD 7. The NH nitrogen atom resonance appears at δ_{N} 86 ppm and the nitro group at δ_{N}

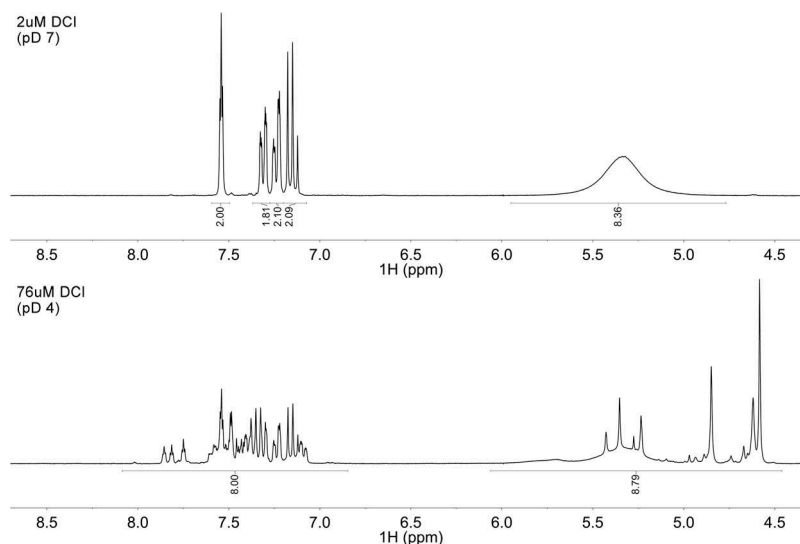


Figure 4. ^1H NMR spectra of compound **1** (*meta*) at pD 7 (top) and pD 4 (bottom) in $\text{DMSO-}d_6$.

373 ppm (Figure S26). Upon addition of acid, the ^1H - ^{15}N HMBC spectra of **3** showed nitrogen atom resonances at δ_{N} 78 ppm and 95 ppm (Figure S27). Similar to **1** and **2**, additional resonances appear likely due to a monoprotonated, and perhaps diprotonated species at lower pH values.

3.5. DFT calculations

DFT calculations were performed for compounds **1–4** at the cam-b3lyp/6-311 + g(d,p)/def2tzv theory level (Figure 5). Frontier molecular orbital contours were calculated for the HOMO-1, HOMO, LUMO and LUMO+1 levels. The heterocyclic cyclooctane ring adopts a stable crown-like conformation at room temperature (**14**) with the two nitrobenzene groups *syn* to the eight-membered heterocyclic ring in agreement with the reported crystal structures of **1** (**11**, **13**) and **2** (**14**). The highest occupied molecular orbitals (HOMO, HOMO-1) describe the charge density of the lone electron pairs. The electrons are predicted to be evenly delocalised over the entire molecule in the case of **1**, **2** and **4**. The largest electron density associated with HOMOs resides primarily on the nitrobenzene moieties, although the heterocyclic ring appears to be involved in HOMO orbitals as well. In the case of **3**, the HOMO is localised on one aromatic ring and the HOMO-1 on the other, with a negligible contribution of the linker. The

lowest occupied molecular orbitals (LUMOs) reside extensively on the nitrophenyl moieties in the cases of **1–4**. The significant difference in the location of the HOMOs and LUMOs clearly illustrates the ICT character.

Electron absorption spectra calculated with the TD-DFT method are in good agreement with the experimental ones (Figure S28). The lowest energy transition involves various combinations of HOMO→LUMO (1,2,3), HOMO-1→LUMO (4) and HOMO→LUMO+1 (1, 2) excitations. An exceptionally high absorptivity of the low energy transition in the case of **2** is attributed to even distribution of the HOMO-1, HOMO, LUMO and LUMO+1 over both nitrophenyl rings. The increased molar absorptivity and higher energy of the lowest excitation results from the characteristics of the *p*-nitrophenyl and *m*-nitrophenyl chromophore are demonstrated with the mono-substituted crown ethers (Figure S29). Simulated UV-visible absorption spectra of the *meta* **1** and *para* **2** monosubstituted crown ethers have λ_{max} at 335 nm (log ϵ 3.20) and 294 nm (log ϵ 4.29).

3.6. Solid-state fluorescence

Compounds **1–3** are yellow powders (Figure 6). We discovered that the heterocycles **1** and **2** exhibit fluorescence in the solid-state (**32**, **33**), while **3** is non-fluorescent. Irradiated with 365 nm UV light, powder **1** emits yellow light and **2** bluish-green light (Figure 6).

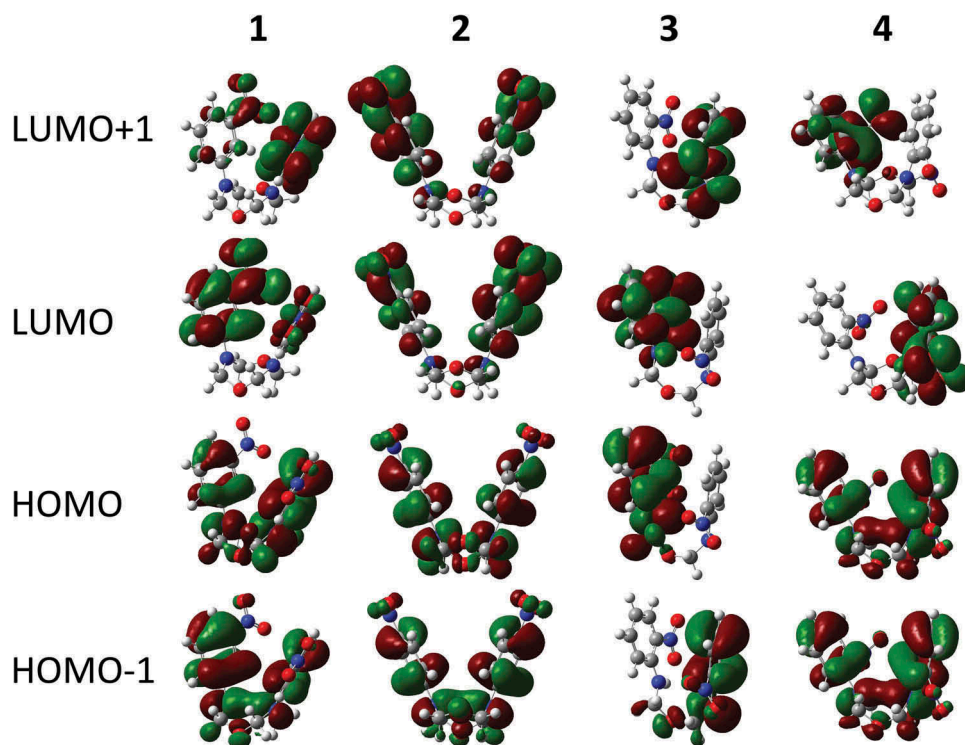


Figure 5. Depiction of the calculated HOMOs and LUMOs for **1–4**.

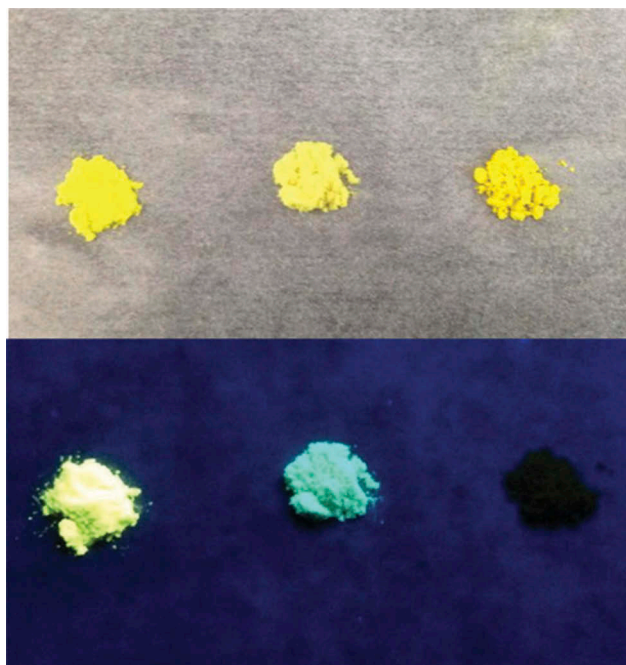


Figure 6. The solids **1–3** (left to right) under room light (top) and irradiated with a 365 nm UV lamp in a dark cabinet (bottom).

The solid-state fluorescence spectra confirm these observations: the emission spectrum of **1** is broadly centred at 542 nm, while the emission spectrum **2** has a maximum at 490 nm and a skewed long tail out to 600 nm (Figure 7). The large Stokes shifts of 172 nm and 139 nm for **1** and **2**, respectively, minimise self-absorption quenching (34). The strong fluorescence in the solid-state is presumably because of reduced intermolecular interactions more typical in solution. The non-planar crown conformation results in weak intermolecular interactions and restricts intramolecular rotation, thus allowing the solids to be emissive (35). In contrast, all three compounds are non-fluorescent in

acetonitrile or 1:1 (v/v) acetonitrile/water. It is hypothesised that hydrogen bonding between the nitro moieties (and the NH in **3**) with acetonitrile or water causes non-radiative vibrational relaxation of the excited state energy.

Further insight comes for the quantum-chemical modelling, which indicates that the electronic structures of **1** and **2** are significantly different than **3** (Figure 5). The HOMO (and also the LUMO) orbitals in compounds **1** and **2** are highly delocalised over the whole molecular frameworks, whereas in **3** only one ring system is involved in the frontier orbitals. It can be hypothesised that this particular arrangement is responsible for the photoluminescence of

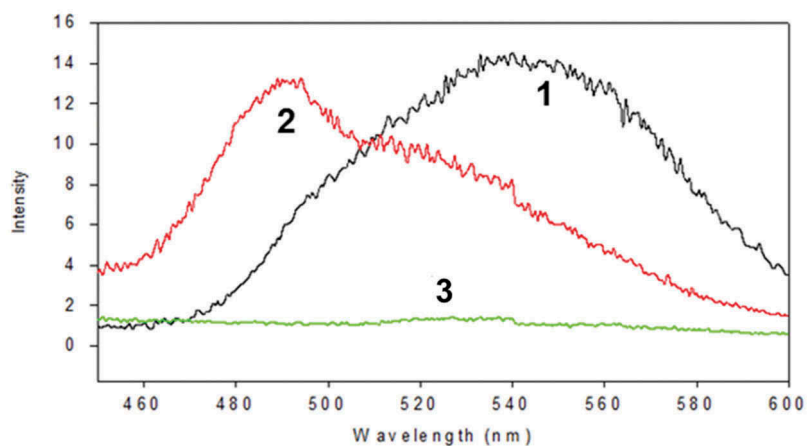


Figure 7. Fluorescence emission spectra of solid samples of **1** (black), **2** (red) and **3** (green) at ambient temperature excited at 370 nm, 351 nm and 406 nm, respectively.

compounds **1** and **2**, in which the electronic structure should efficiently inhibit thermal deactivation of the HOMO-LUMO emissive excited state. On the other hand, the electronic structure of **3** should result in significantly weaker intermolecular interactions in the solid-state, which in turn will be manifested by efficient energy dissipation through vibrational degrees of freedom. This phenomenon is another manifestation of aggregation-induced emission observed in small molecular compounds (35, 36).

4. Conclusions

We synthesised the *meta* and *para*-substituted nitro-diaza-8-crown-4 ethers **1** and **2** by a simple one-pot reaction. The *ortho*-substituted diaza-8-crown-4-ether analogue **4** was not obtained, but rather we obtained *N, N'*-(oxybis(methylene))bis(2-nitroaniline) **3**. The isolation of **3** suggests that the reaction mechanism of **1** and **2** proceeds via a similar common reaction pathway. Proton NMR titration studies provide evidence for protonation and loss of symmetry as is evident from ¹H-¹⁵N NMR correlation studies. No evidence was observed for Li⁺ binding by UV-visible absorption studies. We discovered that **1** and **2** exhibit strong fluorescence in the solid-state with large Stokes shifts, but are not emissive in acetonitrile solution. These results contribute to our knowledge of macrocycles and the development of novel materials with future supramolecular applications (37).

Highlights

- Diaza-8-crown-4-dinitrophenyl ethers were synthesised and analytically characterised.
- The compounds are fluorescent in the solid-state, but not in acetonitrile solution.
- Techniques include 2D ¹H/¹³C/¹⁵N correlation NMR spectroscopy and DFT calculations.

Acknowledgments

Financial support is acknowledged from the University of Malta, the Slovenian Research Agency, the Ministry of Education, Science and Sport of the Republic of Slovenia (program no. P1-0242), the National Science Centre (Poland) within the contract number UMO-2015/17/B/ST8/01783, and EN-FIST Centre of Excellence. DFT calculations were performed at Academic Computer Centre Cyfronet AGH within GRAPHENE4 project. Prof. Robert M. Borg is thanked for his assistance with the NMR experiments. Carl Mallia is thanked for performing some MS measurements.

Disclosure statement

There are no conflicts of interest to declare by the authors.

Funding

This research was funded by the University of Malta, the Slovenian Research Agency [P1-0242] and the Polish National Science Centre [UMO-2015/17/B/ST8/01783].

References

- (1) Li, J.; Yim, D.; Jang, W.-D.; Yoon, J. Recent Progress in the Design and Applications of Fluorescence Probes Containing Crown Ethers. *Chem. Soc. Rev.* **2017**, *46*, 2437–2458. DOI:10.1039/c6cs00619a.
- (2) Gokel, G.W.; Leevy, W.M.; Weber, M.E. Crown Ethers: Sensors for Ions and Molecular Scaffolds for Materials and Biological Models. *Chem. Rev.* **2004**, *104*, 2723–2750. DOI:10.1021/cr020080k.
- (3) Steed, J.W.; First- and Second-Sphere Coordination Chemistry of Alkali Metal Crown Ether Complexes. *Coord. Chem. Rev.* **2001**, *215*, 171–221. DOI:10.1016/S0010-8545(01)00317-4.
- (4) Minkin, V.I.; Dubonosov, A.D.; Bren, V.A.; Tsukanov, A.V. Chemosensors with Crown Ether-Based Receptors. *ARKIVOC.* **2008**, *4*, 90–102.
- (5) Tsukanov, A.V.; Dubonosov, A.D.; Bren, V.A.; Minkin, V.I. Organic Chemosensors With Crown-Ether Groups. *Chem. Heterocycl. Compd.* **2008**, *44*, 899–923. DOI:10.1007/s10593-008-0132-3.
- (6) Valeur, B.; Berberan-Santos, M.N. *Molecular Fluorescence*, 2nd ed.; Wiley-VCH: Weinheim: Germany, **2012**.
- (7) Scheider, H.-J. *Supramolecular Systems in Biomedical Fields*; RSC: Cambridge: UK, **2013**.
- (8) de Silva, A. P. *Molecular Logic-based Computation*; RSC: Cambridge: UK, **2013**.
- (9) Gunnlaugsson, T.; Bichell, B.; Nolan, C. A Novel fluorescent Photoinduced Electron Transfer (PET) Sensor for Lithium. *Tetrahedron. Lett.* **2002**, *43*, 4989–4992. DOI:10.1016/S0040-4039(02)00895-X.
- (10) Gunnlaugsson, T.; Bichell, B.; Nolan, C. Fluorescent PET Chemosensors for Lithium. *Tetrahedron.* **2004**, *60*, 5799–5806. DOI:10.1016/j.tet.2004.04.082.
- (11) Kakanejadifard, A.; Mahmodi, L.; Yari, A.; New Synthesis, M.A. X-Ray Structural Determination, Conformational Analysis and Anomeric Effect Study of 3,7-di(3-nitrophenyl)-1,5-dioxo-3,7-diazacyclooctane. *J. Heterocycl. Chem.* **2006**, *43*, 1695–1697. DOI:10.1002/jhet.5570430642.
- (12) Kolar, G.F.; Schendzielorz, M. 3,7-bis-(4-trifluoromethylphenyl)-1,5,3,7-dioxadiazocine: A Novel Cyclic Product from a Reaction of 4-trifluoromethyl-benzenediazonium Chloride and Methylamine-formaldehyde. *Tetrahedron Lett.* **1985**, *26*, 1043–1044. DOI:10.1016/S0040-4039(00)98507-1.
- (13) Kakanejadifard, A.; Mahmodi, L.; Yari, A. Crystal Structure of 3,7-di(3-nitrophenyl)-1,5-dioxo-3,7-diazacyclooctane. *Anal. Sci.* **2006**, *22*, x163–x164.
- (14) Zhao, -L.-L.; Wan, Y.; Huang, S.-Y.; Chen, L.-F.; Liu, G.-X.; Zhang, W.-L.; Yue, S.-N.; Wu, H. Crystal Structure of 3,7-bis(4-nitrophenyl)-1,5-dioxo-3,7-diazacyclooctane. *Z. Kristallogr.* **2014**, *229*, 23–24.
- (15) Li, L.; Li, H.-Y.; Ren, Z.-G.; Lang, J.-P. Unique Deca- and Tetranuclear Halocuprate(I) Clusters of a Clamplike Ligand: Isolation, Structure, and Luminescence Properties.

- Eur. J. Inorg. Chem.* **2014**, 824–830. DOI:10.1002/ejic.201301433.
- (16) Akhmetova, V.R.; Niatshina, Z.T.; Khabibullina, G.R.; Bushmarinov, I.S.; Borisova, A.O.; Starikova, Z.A.; Korzhova, L.F.; Kunakovaa, R.V. Synthesis, Crystal Structure, and Interconversions of New N-aryl-1,3,5-dithiazinanes, 1,3,5-thiadiazinanes, and 1,5-dithia-3,7-diazacyclooctanes. *Russ. Chem. Bull.* **2010**, *59*, 1002–1009. DOI:10.1007/s11172-010-0196-y.
- (17) Schramm, S.; Weiß, D. *Fluorescent Heterocycles: Recent Trends and New Developments in Advances in Heterocyclic Chemistry*; Academic Press, Elsevier: Cambridge, MA, **2019**, 128, 103–179.
- (18) Basabe-Desmonts, L.; Reinhoudt, D.N.; Crego-Calama, M. Design of Fluorescent Materials for Chemical Sensing. *Chem. Soc. Rev.* **2007**, *36*, 993–1017. DOI:10.1039/b609548h.
- (19) Kamenica, M.; Reddy Kothur, R.; Willows, A.; Anil Patel, B.; Cragg, P.J. Lithium Ion Sensors. *Sensors* **2017**, *7*, 2430–2447. DOI:10.3390/s17102430.
- (20) López, C.; Claramunt, R.M.; Llamas-Saiz, A.L.; Foces-Foces, C.; Elguero, J.; Sobrados, I.; Aguilar-Parrilla, F. Limbach, H. X-ray Diffraction and Solid State NMR Studies of –1,8-bis(dimethylamino)naphthalene and Its Complexes with Picric and Hexafluorophosphoric Acids. *New. J. Chem.* **1996**, *20*, 523–536.
- (21) Barth, T.; Kreiger, C.; Neugebauer, F.A.; Staab, H.A. 1,4,5,8-tetrakis(dimethylamino) Naphthalene: Synthesis, Structure, “proton Sponge” and Electron Donor Properties. *Angew. Chem. Int. Ed.* **1989**, *28*, 86–87.
- (22) Kögel, J.F.; Oelkers, B.; Kovačević, B.; Sundermeyer, J. A New Synthetic Pathway to the Second and Third Generation of Superbasic Biphosphazene Proton Sponges: The Run for the Best Chelating Ligand for A Proton. *J. Am. Chem. Soc.* **2013**, *135*, 17768–17774. DOI:10.1021/ja409760z.
- (23) Staab, H.A.; Saupe, T. “proton Sponges” and the Geometry of Hydrogen Bonds: Aromatic Nitrogen Bases with Exceptional Basicities. *Angew. Chem. Int. Ed.* **1988**, *27*, 865–879. DOI:10.1002/anie.198808653.
- (24) de Silva, A.P.; McClenaghan, N.D. Simultaneously Multiply-Configurable or Superposed Molecular Logic Systems Composed of ICT (internal Charge Transfer) Chromophores and Fluorophores Integrated with One- or Two-Ion Receptors. *Chem. Eur. J.* **2002**, *8*, 4935–4945. DOI:10.1002/1521-3765(20021104)8:21<4935::AID-CHEM4935>3.0.CO;2-2.
- (25) de Silva, A.P.; Magri, D.C. Optical Sensing and Switching with Designed Molecules. *Chimia* **2005**, *59*, 218–221. DOI: 10.2533/000942905777676579.
- (26) de Silva, A.P.; Gunaratne, H.Q.N.; Lynch, P.L.M.; Patty, A. J.; Spence, G.L. Luminescence and Charge Transfer. Part 3. The Use of Chromophores with ICT (Internal Charge Transfer) Excited States in the Construction of Fluorescent PET (Photoinduced Electron Transfer) pH Sensors and Related Absorption pH Sensors with Aminoalkyl Side Chains. *J. Chem. Soc. Perkin Trans 2* **1993**, 1611–1616.
- (27) Frisch, M. J.; Trucks, G. W.; Schlegel, H. B.; Scuseria, G. E.; Robb, M. A.; Cheeseman, J. R.; Scalmani, G.; Barone, V.; Mennucci, B.; Petersson, G. A.; Nakatsuji, H.; Caricato, M.; Li, X.; Hratchian, H. P.; Izmaylov, A. F.; Bloino, J.; Zheng, G.; Sonnenberg, J. L.; Hada, M.; Ehara, M.; Toyota, K.; Fukuda, R.; Hasegawa, J.; Ishida, M.; Nakajima, T.; Honda, Y.; Kitao, O.; Nakai, H.; Vreven, T.; Montgomery Jr., J.A. ; Peralta, J. E.; Ogliaro, F.; Bearpark, M.; Heyd, J. J.; Brothers, E.; Kudin, K. N.; Staroverov, V. N.; Kobayashi, R.; Normand, J.; Raghavachari, K.; Rendell, A.; Burant, J. C.; Iyengar, S. S.; Tomasi, J.; Cossi, M.; Rega, N.; Millam, J. M.; Klene, M.; Knox, J. E.; Cross, J. B.; Bakken, V.; Adamo, C.; Jaramillo, J.; Gomperts, R.; Stratmann, R. E.; Yazyev, O.; Austin, A. J.; Cammi, R.; Pomelli, C.; Ochterski, J. W.; Martin, R. L.; Morokuma, K.; Zakrzewski, V. G.; Voth, G. A.; Salvador, P.; Dannenberg, J. J.; Dapprich, S.; Daniels, A. D.; Farkas, O.; Foresman, J. B.; Ortiz, J. V.; Cioslowski, J.; Fox, D. J. *Gaussian 09, Rev. A.02*; Gaussian, Inc.; Wallingford CT, **2009**.
- (28) Yanai, T.; Tew, D.P.; Hardy, N.C. A New Hybrid Exchange–Correlation Functional Using the Coulomb-attenuating Method (CAM-B3LYP). *Chem. Phys. Lett.* **2004**, *393*, 51–57. DOI: 10.1016/j.cplett.2004.06.011.
- (29) Cardona, M.A.; Makuc, D.; Szaciłowski, K.; Plavec, J.; Magri, D.C. Water-Soluble Colorimetric Amino[bis-(ethanesulfonate)] Azobenzene pH Indicators: A UV–Vis Absorption, DFT, and ¹H–¹⁵N NMR Spectroscopy Study. *ACS Omega*. **2017**, *2*, 6159–6166. DOI: 10.1021/acsomega.7b00887.
- (30) Farrugia, K.N.; Makuc, D.; Podborska, A.; Szaciłowski, K.; Plavec, J.; Magri, D.C. Colorimetric Naphthalene-Based Thiosemicarbazide Anion Chemosensors with an Internal Charge Transfer Mechanism. *Eur. J. Org. Chem.* **2016**, *25*, 4415–4422. DOI:10.1002/ejoc.201600509.
- (31) Farrugia, K.N.; Makuc, D.; Podborska, A.; Szaciłowski, K.; Plavec, J.; Magri, D.C. UV-visible and ¹H–¹⁵N NMR Spectroscopic Studies of Colorimetric Thiosemicarbazide Anion Sensors. *Org. Biomol. Chem.* **2015**, *13*, 1662–1672. DOI:10.1039/c4ob02091j.
- (32) Da Silveira Santos, F.; Goedel Medeiros, N.; Ferreira Affeldt, R.; Da Costa Duarte, R.; Moura, S.; Severo Rodembusch, F. Small Heterocycles as Highly Luminescent Building Blocks in the Solid State for Organic Synthesis. *New. J. Chem.* **2016**, *40*, 2785–2791. DOI:10.1039/C5NJ02943K.
- (33) Carayon, C.; Fery-Forgues, S. 2-phenylbenzoxazole Derivatives: A Family of Robust Emitters of Solid-state fluorescence. *Photochem. Photobiol. Sci.* **2017**, *16*, 1020–1035. DOI:10.1039/c7pp00112f.
- (34) Maeda, C.; Todaka, T.; Ueda, T.; Ema, T. Color-Tunable Solid-State Fluorescence Emission from Carbazole-Based BODIPYs. *Chem. Eur. J.* **2016**, *22*, 7508–7513. DOI:10.1002/chem.201505150.
- (35) Hong, Y.; Lam, J.W.Y.; Tang, B.Z. Aggregation-Induced Emission. *Chem. Soc. Rev.* **2011**, *40*, 5361–5388. DOI:10.1039/c1cs15113d.
- (36) Mei, J.; Leung, N.L.C.; Kwok, R.T.K.; Lam, J.W.Y.; Tang, B.Z. Aggregation-Induced Emission: Together We Shine, United We Soar! *Chem. Soc. Rev.* **2015**, *115*, 11718–11940.
- (37) Zwoliński, K.M.; Eilmel, J. Design, Synthesis and Spectroscopic Properties of Crown Ether-capped Dibenzotetraaza[14]annulenes. *Beilstein. J. Org. Chem.* **2019**, *15*, 617–622. DOI:10.3762/bjoc.15.57.